Breakout character of islet amyloid polypeptide hydrophobic mutations at the onset of type-2 diabetes

Rafael B. Frigori
Universidade Tecnológica Federal do Paraná (UTFPR) and
*Rua Cristo Rei 19, CEP 85902-490, Toledo (PR), Brazil.**
(Dated:)

Toxic fibrillar aggregates of Islet Amyloid PolyPeptide (IAPP) appear as the physical outcome of a peptidic phase-transition signaling the onset of type-2 diabetes mellitus in different mammalian species. In particular, experimentally verified mutations on the amyloidogenic segment 20-29 in humans, cats and rats are highly correlated with the molecular aggregation propensities. Through a microcanonical analysis of the aggregation of IAPP_{20-29} isoforms, we show that a minimalist one-bead hydrophobic-polar continuum model for protein interactions properly quantifies those propensities from free-energy barriers. Our results highlight the central role of sequence-dependent hydrophobic mutations on hot spots for stabilization, and so for the engineering, of such biological peptides.

arXiv:1411.1672v1 [q-bio.BM] 5 Nov 2014

I. INTRODUCTION

Diabetes mellitus type 2 (DM-II) is a metabolic disorder characterized by hyperglycemia, due to insufficient insulin secretion from Pancreatic $\beta-$cells in the setting of insulin resistance. Beyond the yearly premature death of about 4 million people worldwide, diabetes also implies a high prevalence of health complications as stroke (68%), high blood pressure (67%), blindness (28.5%), kidney disease (44%), neuropathies and amputation (60%) [1]. Its outbreak is correlated to genetic factors associated to a sedentary modern lifestyle, which implies that an increasing global diabetes epidemic is underway. In 2010 there was 285 million cases in adults worldwide, with an estimated annual health care economic burden of USD 376 billion [2]. Such scenario urges for deepening the pathophysiological understanding of the DM-II onset.

In this vein, since the pioneering study by Westermark *et* al. in the 1990's [3], it has become increasingly known that Amylin (or IAPP), a small 37-residues putative polypeptide (small protein) hormone also produced by pancreatic $\beta-$cells, constitutes most fibrillar amyloid deposits seen in the islets of Langerhans in diabetic humans [4] and other mammals. Further experimental studies [5] have demonstrated that fibrillar amylin is toxic to insulin-producing $\beta-$cells, so inducing an enhanced loss of islet cells characteristic of type-2 diabetes. In addition, the propensity for islet amyloid deposition is specie-specific, a property mostly due to mutations in hot spots as the IAPP_{20-29} segments [3], which correlates positively with the molecular toxicity of IAPP isoforms in humans (hIAPP) and cats (cIAPP), while most rodents (rIAPP) never develop such a syndrome. Thus, the toxicity of amylin seems strikingly similar to the effects observed in other well-known amyloidosis [6], as the Alzheimer's disease and spongiform encephalopathies.

Generally, while the ability of polypeptides on forming such amyloid structures is considered as a common feature of such molecular chains, the propensity to do so varies markedly between different sequences. Therefore, aggregation rates correlates [7] with the physicochemical properties of those molecules as charge, secondary-structure and hydrophobicity [8]. Hence, peptide proneness for aggregation can be related to eventual misfoldings [6], which is explained by the thermostatistical theory of the energy landscape of protein folding [9]. In accordance with which realistic models of proteins are minimally frustrated heteropolymers that reach the lowest-energy (native, or folded) state through an ensemble of intermediate self-organizing structures, guided by a rugged funnel-like energy landscape. Although details on the native conformation of proteins may depend on specificities of each energetic potential, coarse-grained models for amino acid interactions, where more or less profound simplifications are made, have provided powerful insights on the aggregation mechanisms underlying degenerative diseases [10].

Hence peptides are small proteins composed by inhomogeneous sequences of amino acids (residues), they constitute a class of finite systems inherently far from the thermodynamic limit, to whose description the thermostatistical postulate of ensemble equivalence does not hold. Thereby, the original microcanonical formulation of Statistical Mechanics [11], designed to be rigorously valid even for systems having finite degrees of freedom, turns to be most appropriate for studying phase-transitions on proteins as their folding [12] and aggregation [13]. In this approach, starting from the density of states $g(E)$, the celebrated Boltzmann entropy $S(E) = k_B \ln g(E)$ is the solely responsible to yield thermodynamical quantities, as the microcanonical temperature $T(E)$ and the specific heat $C_V(E)$. Additionally, free energies $H(E)$ can be also straightforwardly accessed by taking Legendre transforms. However, in this context, it deserves to be noted that $S(E)$ may become a convex function of E, as during first-order phase transitions, which induces peculiar thermodynamic behaviors as backbendings on $T(E)$, negative values of $C_V(E)$ and appearance of energetic barriers on free energies ΔH [11].

In this article we show how, through a microcanon-

* frigori@utfpr.edu.br

ical analysis from multicanonical Monte Carlo simulation data [14], the ratios among aggregation propensities of IAPP isoforms can be recovered from the energetic barriers emerging in the vicinity of the (first-order) phase transitions of a simple coarse-grained hydrophobic-polar model for protein interactions [13, 15]. Our results weakly depend on a input scale [16] and nicely agree with widely-accepted heuristic predictors able to reproduce *in vitro* as well as *in vivo* experimental data [17, 18]. In the spirit of [19], we conclude that even a two-letter code can discriminate amyloidogenic characters on primary sequences of IAPP. This corroborates with an underlying rationale relating the thermodynamic aspects associated to sequence-dependent hydrophobic mutations with the (kinetic) aggregation rates of peptides [7], so that more aggregation prone sequences also form pathogenic aggregates faster.

The work is organized as follows, in Section II an effective one-bead hydrophobic-polar continuum model for describing protein interaction and aggregation is introduced. The Section III is devoted to the algorithmic setup and numerical results emerging from our multicanonical simulations of IAPP_{20-29} segments of several mammalian species. In Section IV free energies are exploited to connect thermodynamic and kinetic aspects of peptide aggregation. There, we propose a method to evaluate relative aggregation propensities of proteins, a rationale inspired in spectral predictions by universality-related theories. Those results are validated by confrontation with well-established heuristic online aggregation-propensity estimators. The Section V summarizes our results confronting them to recent all-atom simulations, so highlighting future research perspectives. Still, we devote an Appendix to numerical error estimates in microcanonical data-analysis.

II. AN EFFECTIVE MODEL FOR PROTEIN AGGREGATION

Hydrophobic forces are not fundamental forces of Nature [8]. Despite of it, by considering their central role on the assembling of three-dimensionally ordered tertiary structures during protein folding, while keeping high simplicity standards on molecular modeling, we have adopted a coarse-grained (one-bead) hydrophobic-polar model for proteins [15, 20]. There the target protein is mapped, depending on the hydrophobic character of the constituents lying on its primary sequence of amino acids, on a heteropolymer made of hydrophobic (A) or polar (B) pseudo-atoms (beads).

Those monomers so replace the original residues on their $\alpha-$carbon positions occupied at the same peptidic backbone structure. The interaction energy ($\mathcal{H}$) among the N pseudo-atoms in the chain is given by

$$\mathcal{H} = \frac{1}{4}\sum_{k=1}^{N-2}\left(1-\cos\alpha_k\right) + 4\sum_{i=1}^{N-2}\sum_{j=i+2}^{N}\Phi\left(r_{ij};C_{\sigma_i,\sigma_j}\right). \tag{1}$$

Where the first term describes the virtual bending angle ($0 \leq \alpha_k \leq \pi$) between three successive monomers, while the second term

$$\Phi\left(r_{ij};C_{\sigma_i,\sigma_j}\right) = \left[r_{ij}^{-12} - C\left(\sigma_i,\sigma_j\right) r_{ij}^{-6}\right] \tag{2}$$

provides a long-distance (r_{ij}) pairwise-interaction between residues i and j, depending on their hydrophobic character $\sigma \in \{A,B\}$. That is

$$C\left(\sigma_i,\sigma_j\right) = \begin{cases} +1 & \sigma_i,\sigma_j = A \\ +1/2 & \sigma_i,\sigma_j = B \\ -1/2 & \sigma_i \neq \sigma_j \end{cases}. \tag{3}$$

Then, attractive ($C_{A,A}, C_{B,B}$) or repulsive ($C_{A,B}, C_{B,A}$) forces will naturally emerge from primary sequences of amino acids once they are properly translated on a two-letter code by a hydrophobic scale [16] used as a lexicon.

Hence aggregation is a many-body effect, it shall be provided by a multi-protein potential [13]

$$\Psi_{multi-prot.} = \sum_{k=1}^{M}\left[\mathcal{H}_k + \sum_{l>k}\sum_{i,j=1}^{N}\Phi\left(r_{l_i k_j};C_{\sigma_{l_i},\sigma_{k_j}}\right)\right]. \tag{4}$$

Thus, in addition to the intra-protein energy $\mathcal{H}_k$, from Eq.(1), there is a contribution from all pairs of residues (l_i, k_j) located in different proteins (l or k) of a set of M proteins. It deserves to be noted that in such coarse-grained model long-range forces are only due to hydrophobic/polar effective interactions, so any interacting pair (i,j) of pseudo-atoms in the system is equally described by the same C_{σ_i,σ_j} coupling constants (Eq. 3). It clearly is a simplifying hypothesis inspired on mean-field descriptions, justified as a leading-order approach, in the sense of a renormalization group analysis.

III. SIMULATIONS AND THERMODYNAMIC RESULTS

To obtain the microcanonical entropy associated to the aggregation of segments of IAPP isoforms, and so their caloric and specific-heat curves, we have focused on performing Monte Carlo multicanonical (MUCA) simulations [14] of multiple (amyloidogenic) IAPP_{20-29} segments. Coefficients a_k and b_k in multicanonical weights $\omega_{muca}\left(E_k\right) = e^{b_k E_k - a_k}$ can be determined by an iterative procedure using energy histograms $H_{muca}\left(E\right)$ for energies E_k in a interval $E = [E_0, \ldots, E_{max}]$. Thus, in the beginning, one sets $\omega^0_{muca}\left(E\right) = 1$ for all energies, which is used to run a usual METROPOLIS simulation

to build $H^0_{muca}(E)$. The next guess for the weights in the simplest update scheme is given by $\omega^1_{muca}(E) = H^0_{muca}(E)/\omega^0_{muca}(E)$. Such iterative procedure is then repeated till the energy histogram converges to a "flat" distribution. In our implementation we have employed accumulated error-weighted histograms, so statistics for weights estimation improves every run, while convergence is ensured by Berg's weight recursion [21].

Once MUCA weights are established, they provide a good piecewise approximation to the microcanonical entropy $S_{micro}(E_k) = b_k E_k - a_k$. Then, numerical derivatives of the entropy can be employed to compute thermodynamic quantities of interest [11], as the microcanonical caloric curve

$$\beta(E) \equiv T^{-1}(E) = \frac{\partial S}{\partial E}, \tag{5}$$

the microcanonical specific heat

$$C_V(E) = \frac{dE}{dT} = -\left(\frac{\partial S}{\partial E}\right)^2 \left(\frac{\partial^2 S}{\partial E^2}\right)^{-1}, \tag{6}$$

and the free energy

$$H(E) = E - \left(\frac{\partial S}{\partial E}\right)^{-1} S(E). \tag{7}$$

In particular, we have applied the finite differences method with central derivatives and stability constraints to fix their maximal kernel sizes.

After the original protein sequences of amyloidogenic IAPP_{20-29} segments were mapped on AB-model (respectively, on the second and third column of Tab. 1) through an hydrophobicity scale [16], simulations with different ensembles — having up to eight copies — of interacting peptides were done. For the Monte Carlo evolution of a set having N pseudo-atoms we performed 10^3 MUCA iterations, in a total of about $3N \times 10^9$ updates, by mixing spherical-cap [13] and pivoting [22] algorithms. The independence of our results with energy-bin size — i.e. $\triangle E = E_{k+1} - E_k$ — and finite-box effects were checked to certify for data robustness (see Appendix). In particular, as containers we have used spherical boxes (of radius $R \simeq 100$), whose interior was initially populated with stretched and randomly positioned peptides. The Bolztmann constant was taken as $k_B = 1$ and distances of nearest-neighbor residues was normalized to unit. For convenience we use intensive units for the system energy $\varepsilon = E/N$. Error-bars were computed by data-blocking and resampling techniques.

The data analysis of our simulations shows that [see Fig.(1) and Tab.(1), for a summary] as it is usually observed in first-order phase transitions, described under the microcanonical formalism of statistical mechanics [11], negative specific heats are seen on regions where the microcanonical entropy presents a convex intruder. Inside such regions, delimited by a minimum energy bellow whom proteins are completely aggregated ($\varepsilon_{min} = \varepsilon_{agg.}$) and a maximal one above which aggregates dissolve by

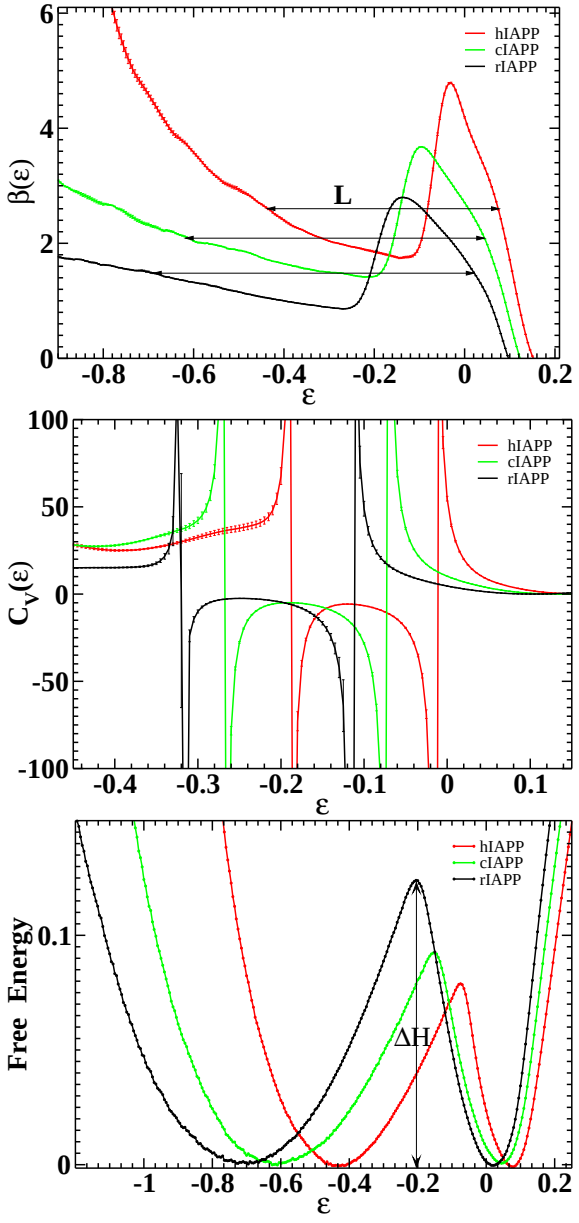

Figure 1. (Color online) The thermodynamic behavior of segments of Amylin isoforms as cIAPP in green (light gray), rIAPP in black (black) and hIAPP in red (dark gray) as a function of energy (E) per residue $\varepsilon = E/N$. Upper Panel: caloric curve. Center Panel: microcanonical specific heat. Lower Panel: the Helmholtz free-energy barrier (error-bars are smaller than the circles).

Peptide	Sequence	AB-Sequence	β_c	$\triangle H$	L
hIAPP_{20-29}	SNNFGAIL**SS**	BBBABAAA**BB**	2.60(2)	0.079(1)	0.520(5)
cIAPP_{20-29}	SNNFGAIL**SP**	BBBABAAA**BA**	2.09(1)	0.092(1)	0.636(10)
rIAPP_{20-29}	SNNLGPVL**PP**	BBBABAAA**AA**	1.48(1)	0.124(1)	0.698(10)

Table I. The inverse-temperature at aggregation β_c, the free-energy barriers $\triangle H$ and latent specific-heat L, for human (hIAPP), cat (cIAPP) and rat (rIAPP) segments of Amylin isoforms obtained by microcanonical analysis from MUCA simulations.

fragmentation ($\varepsilon_{max} = \varepsilon_{frag.}$), the caloric curves $\beta(\varepsilon)\times\varepsilon$ display signals of thermodynamic metastability. Those configurations induce a forbidden region for the canonical ensemble, which entails the need of applying a well-known Maxwellian prescription around the (inverse) temperature of transition β_c, whereas the (upper) A_+ and (lower) A_- areas of the bumps formed by the backbending of $\beta(\varepsilon_{frag.} < \varepsilon < \varepsilon_{agg.}) \neq \beta_c$ becomes equal. As a result, it implies not only on the inequivalence of canonical and microcanonical ensembles during the phase transition, once a bijective mapping between the system temperature and energy is only possible for $\varepsilon < \varepsilon_{agg.}$ or $\varepsilon > \varepsilon_{frag.}$, but also on the arising of a latent heat defined by $L = \varepsilon_{frag.} - \varepsilon_{agg.}$.

After evaluating β_c for the aforementioned Amylin segment isoforms of humans $\beta_{c-hIAPP} = 2.60\,(2)$, cats $\beta_{c-cIAPP} = 2.09\,(1)$ and rats $\beta_{c-rIAPP} = 1.48\,(1)$, we found the foregoing description as appropriate for those regions of phase-transition. To know, negative microcanonical specific heats, and so latent (canonical) heats, can be seen inside $\varepsilon_{hIAPP} = [-0.439, 0.008]$ for humans, cats: $\varepsilon_{cIAPP} = [-0.595, 0.041]$ and rats: $\varepsilon_{rIAPP} = [-0.683, 0.015]$. Among such isoforms, hIAPP has in fact the smallest latent heat of transition $L_{hIAPP} = 0.520$ and the lowest energetic barrier $\triangle H_{hIAPP} = 0.079\,(1)$ for aggregation, which is followed by cIAPP where $L_{cIAPP} = 0.636$ and $\triangle H_{cIAPP} = 0.092(1)$, and rIAPP with $L_{rIAPP} = 0.698$ and $\triangle H_{rIAPP} = 0.124(1)$. Latent heat is a consequence of the free-energy barrier and prevents the system from moving to a stable configuration in the new phase. Therefore, the smaller the latent heat, the higher the probability that a spontaneous thermal fluctuation will give rise to the aggregate phase.

IV. AGGREGATION PROPENSITIES

Since polypeptide aggregation is an example of nucleated polymerization reaction where from a tiny nucleating event larger aggregates grows up into fibrillar structures, the efficiency of these reactions is related to the rate of aggregation [23]. By the Arrhenius equation it is also widely-known [24] that thermodynamic and kinetic properties are connected by the relation $\Delta H = N_A \beta^{-1} \ln K_D$, where $\triangle H$ is the free energy of aggregation, N_A is the Avogadro number and K_D is the dissociation equilibrium constant related to the ratio of dissociation(k_-)/association(k_+) rates in a two-state binding reaction. Higher aggregation propensities (henceforth named "z") are therefore associated to lower values of K_D, or equivalently, to faster association rates, which is thermodynamically favoured by smaller energetic barriers (so $z \propto \Delta H^{-1}$). This implies on a causal relation, experimentally already observed for variants of $\beta-$amyloid proteins, where the more stable aggregates are also the ones that aggregates more readily [25]

Thus, in principle, one would expect that accurate information about phase transitions as protein aggregation could be obtained only by atomic-level simulations. However, in the vicinity of critical phase transitions — where correlation lengths become greater than characteristic system sizes — different physical systems can exhibit the same universal behavior. Which constitutes a powerful predictive tool of statistical mechanics. For instance, in the context of protein folding, an effective lattice gauge field theory built only upon symmetry arguments [26] were shown to be, in the sense of the compactness index, in the same universality class of proteins deposited in the Protein Data Bank. Despite of the conceptual simplicity of such model, even the secondary structural motifs of all studied proteins could be reconstructed with a backbone RMS accuracy of about $1\overset{\circ}{A}$ [27]. This success arguably relies on the fact that on such field-theoretic language the formation of protein loops can be described by topological domain-wall solitons, interpolating among ground states given by $\alpha-$helices and $\beta-$strands, despite of local details of their Hamiltonian interactions [27].

In a somehow similar scenario, the long-standing conjecture by Svetitsky and Yaffe [28], relating the magnetic phase transitions in $d-$dimensional Z_N Potts-like spin models and deconfinement in $SU(N)$ quantum gauge theories in $(d+1)-$dimensions, have been widely verified beyond usual realms of critical exponents and universal amplitude ratios (see [29], and references therein). In fact, through universality, the emergence of bound states in the broken symmetry phase of spin systems was unveiled to be a phenomenon closely related to the formation of a Quark-Gluon Plasma (QGP) [29], where the gluonic potential among static quark charges becomes short-ranged by acquiring a spectrum of effective Debye-screening masses (m_D). There, changes in the system free energy $H(r,T)$ at (asymptotic) large quark-distances are given by $\triangle H_\infty(T) \equiv \lim_{r\to\infty} H(r,T) \propto m_D(T)$ [30]. Regardless of the fact that those excited spectra are not universal, the ratios computed among their mass-states (in the same channel) were shown to be [29]. More surprisingly, even when phase transitions are weak first-order — as it happens in quenched $SU(3)$ QCD and Z_3-Potts model — those respective ratios computed from both (approximate) universality-related theories still coincide up to a precision of 30% [31].

Inspired on those concepts, we propose that the aggregation propensities z_a and z_b for peptidic isoforms a and b may be combined to form a dimensionless ratio r_{ab} who shall depends only on relative changes in the system free energy, it is $r_{ab} = z_a \cdot z_b^{-1} = [\triangle H_a]^{-1} \cdot [\triangle H_b]$. Thenceforth, by performing such analysis over the data obtained from our AB-Model simulations [see Tab.(1)], we have obtained relative aggregation propensities explicited by the following ratios $r_{hc}^{AB} \simeq 1.16\,(2)$, $r_{hr}^{AB} \simeq 1.57\,(2)$ and $r_{cr}^{AB} \simeq 1.35\,(2)$. How far one can lead such argument is a matter for numerical verification, so we intend to cross check our results with alternative methods for further validation.

To accomplish this very end, we have chosen two different heuristic algorithms designed to accurately pre-

dict — after being properly calibrated — the aggregation propensities z of a plethora of *in vitro* (z_{Agg}) as well as *in vivo* (z_{Scan}) experiments. First, we evaluated the so-called z_{Agg} score from Zyggregator [17], a phenomenological model that incorporates both *intrinsic* factors of peptides as hydrophobicity, charge, and the propensity of the polypeptide chain to adopt $\alpha-$helical or $\beta-$sheet structures as well as *extrinsic* ones (physicochemical properties related to the environment). Consequently, higher scores means that a sequence is more suitable to aggregation. This approach has resulted for the primary sequences of IAPP the following aggregation-propensity scores $z_{Agg.}^{hIAPP} = 1.30(9)$, $z_{Agg.}^{cIAPP} = 1.05(15)$ and $z_{Agg.}^{rIAPP} = 0.92(13)$. So, computing the ratios among those scores — such that $r_{ab}^{z_{Agg}} = \left[z_{Agg}^{a}\right] \cdot \left[z_{Agg}^{b}\right]^{-1}$ — has produced these relative aggregation propensities $r_{hc}^{z_{Agg}} \simeq 1.24\,(19)$, $r_{hr}^{z_{Agg}} \simeq 1.41\,(22)$ and $r_{cr}^{z_{Agg}} \simeq 1.14\,(23)$.

On the other hand, AGGRESCAN [18] is an online aggregation-propensity predictor solely based on *in vivo* experimental data. It assumes that short and specific segments of peptidic sequences modulate protein aggregation and, as an outcome, the effects of genetic mutations on aggregation propensities (of an input sequence) can be precisely predicted from comparisons with a databank. The generated score z_{Scan} for Amylin isoforms are given by $z_{Scan}^{rIAPP} = -8.80$, $z_{Scan}^{cIAPP} = -6.60$ and $z_{Scan}^{hIAPP} = -5.60$, where more negative values imply naturally less aggregation prone sequences. After due normalization, the ratios among relative aggregation propensities are analogously obtained $r_{hc}^{z_{Scan}} \simeq 1.18$, $r_{hr}^{z_{Scan}} \simeq 1.57$ and $r_{cr}^{z_{Scan}} \simeq 1.39$.

Thus, our results for r^{AB} are compatible (within less than 1 stdv.) with ratios of aggregation-propensities estimated from *in vitro* phenomenological methods ($r^{z_{Agg}}$), whereas when compared to ratios obtained from *in vivo* data-based methods ($r^{z_{Scan}}$) discrepancies were lower than 2%, in an even better agreement. Such numbers reinforce not only our previous working hypothesis that hydrophobic mutations play an essential hole on the determination of peptide stability, but also that substitutions are strongly sequence-dependent on the so-called protein hot spots, as is the case of IAPP_{20-29} [3].

More interestingly, from a thermodynamic viewpoint, the height of energetic barriers are associated not only to nucleation rates but also to reaction kinetics, as the required time (time-lag τ_c) for reaching steady-state nucleation that is $\tau_c \propto \exp(\beta \triangle H)$ [32]. From such perspective, less stable molecular isoforms of IAPP — i.e., the ones with smaller latent heats, or equivalently, having lower energetic barriers — would induce a quicker production of IAPP aggregates on mammalian pancreas, as is the case of humans (hIAPP) and cats (cIAPP). While for more stable isoforms, as of rats (rIAPP), the huge time-scales associated would be a deterrent pathophysiological factor for the onset of Diabetes II.

This could lead to an alternative pathway for *in silico* designing of artificial peptides aiming to act as adjuncts for DM-II, under the constraint that they must keep biocompatibility with usual Amylin, while should avoid its notorious metastability. For instance, till recently, these features could be found just in Pramlintide [33], an experimentally screened rat-modified version of IAPP.

V. CONCLUDING REMARKS

In this article, we have shown that by performing microcanonical analysis of a simple coarse-grained hydrophobic-polar heteropolymer model for aggregation of proteins, who are mapped by a hydrophobicity scale in a two-letter code lexicon, the onset of type-2 diabetes Diabetes mellitus in different mammalian species correlates with aggregation propensities derived from the thermodynamics of first-order aggregation transitions of specific segments of Amylin isoforms (IAPP_{20-29}). The (almost) universal ratios among such aggregation propensities extracted from our *ab initio* multicanonical simulations were in nice agreement with well-established heuristic predictors. It corroborates to a rationale underlying the thermodynamics of sequence-dependent hydrophobic mutations on peptides (hot spots) with the kinetic aspects of their associated polymerization reactions, hence more aggregation prone (i.e. less stable) sequences shall aggregate faster. These findings may bring potentially new insights for designing and screening peptides as adjuncts for DM-II therapy from *in silico* methods.

Still, such conclusions are confirmed by recent studies, where some groups have been succeed on simulating the aggregation processes of IAPP through Molecular Dynamics (MD) techniques using all-atoms potentials with implicit [34] or explicit solvent [35]. For instance, in [35] authors have investigated the aggregation of decamers of hIAPP and rIAPP in double layers. Then, by comparing average intermolecular distances (R) and the van der Waals interaction energies ($\triangle H$) among those rIAPP and hIAPP aggregates it was found that $R_{hIAPP} \simeq (3.7 \pm 0.3)\,\mathring{A}$ and $R_{rIAPP} \simeq (4.2 \pm 0.7)\,\mathring{A}$, while $\triangle H_{hIAPP} = (-233.6 \pm 24.7)\,kcal/mol$ and $\triangle H_{rIAPP} = (-326.5 \pm 64.5)\,kcal/mol$. So, it has been arguably verified that differences in stability between those IAPP isoforms — concerning their molecular compactness index and free energy differences — is most likely due to the existence of β-sheet breaking (hydrophobic) Prolines in rIAPP_{25-29} segment, which is missing in hIAPP_{25-29}.

Surprisingly enough, by using the aforementioned data in our present methodology one finds a relative aggregation propensity $r_{hr}^{MD} \simeq 1.39\,(31)$, which is in remarkable aggreement with our result $r_{hr}^{AB} \simeq 1.57\,(2)$. This provides not only a compelling verification for the correctness of our working hypothesis in Section IV, which relies on general universality-based arguments, but also constitutes a further evidence for the breakout character of IAPP hydrophobic mutations at the onset of type-2 Diabetes. Finally, it would be very interesting to investigate how slightly extended letter codes for amino acids

(as in [36]), together with more refined coarse-grained models [10, 19], may impact on quantitative predictions of aggregation propensities of other mammalian IAPP isoforms eventually able to work as natural aggregation-deterrents.

ACKNOWLEDGMENTS

The author thanks Jorge Chahine, Leandro G. Rizzi, Nelson A. Alves and Rinaldo W. Montalvão for useful discussions. We also thank the anonymous referees by a highly constructive job. This project was partially funded by the Brazilian agency CNPq. Simulations were performed on the SGI-Altix at CENAPAD-Unicamp.

APPENDIX

In a microcanonical simulation [11] the entropy $S(E_k) = b_k E_k - a_k$ is estimated as a piecewise function, hence energies are discretized in M bins: $\triangle E = E_{k+1} - E_k$. Thus, $S(E)$ is build up through a recursive process, where energy histograms are accumulated during a serie of Monte Carlo runs [14, 21]. After the entropy is obtained, up to a good numerical precision, numerical derivatives can be employed to direct extract the system thermodynamics Eq.(5), Eq.(6), Eq.(7). Therefore, in such simulations, not only statistical and finite (box) size-effects are important factors to ensure for data robustness, but also evaluating the most appropriate energy bin-size and checking against finite-difference instabilities.

As an illustration we provide the output of some data-analysis we have performed as preliminary simulations to set parameters for our production runs. The system we have chosen is a small ensemble consisting of two hIAPP_{20-29} molecules ($N = 2 \times 10$), which was simulated by methods already described in Section III, and whose parameters — energy-bin sizes $\triangle E$, the radius of the spherical container R and kernel-size of numerical derivatives dE — were systematically varied. For every MUCA run we have accumulated statistics during 10^6 Monte Carlo evolution steps, a summary of our results is given in Fig. (2). Error bars were computed by usual data-blocking and resampling methods [37]

Concerning our checks for energy-bin sizes, for each value of $\triangle E$ we have initially evaluated the ground-state E_{ground} for the dimerization of hIAPP_{20-29} during 350 MUCA runs. There we have obtained $E_{ground} = \{-18.69, -18.23, -17.84, -20.32\}$ respectively for $\triangle E = \{0.1, 0.2, 0.5, 1.0\}$. Thus, while larger values of $\triangle E$ apparently favour sampling lower-energy states — most likely due to improved signal-to-noise ratios — they provide us with a coarser mesh that prevents smooth numerical derivatives of $S(E)$ to be safely employed around the transition. This fact is demonstrated by the caloric curve $\beta(\varepsilon) \times \varepsilon$ — where $\varepsilon = E/N$ — depicted in the

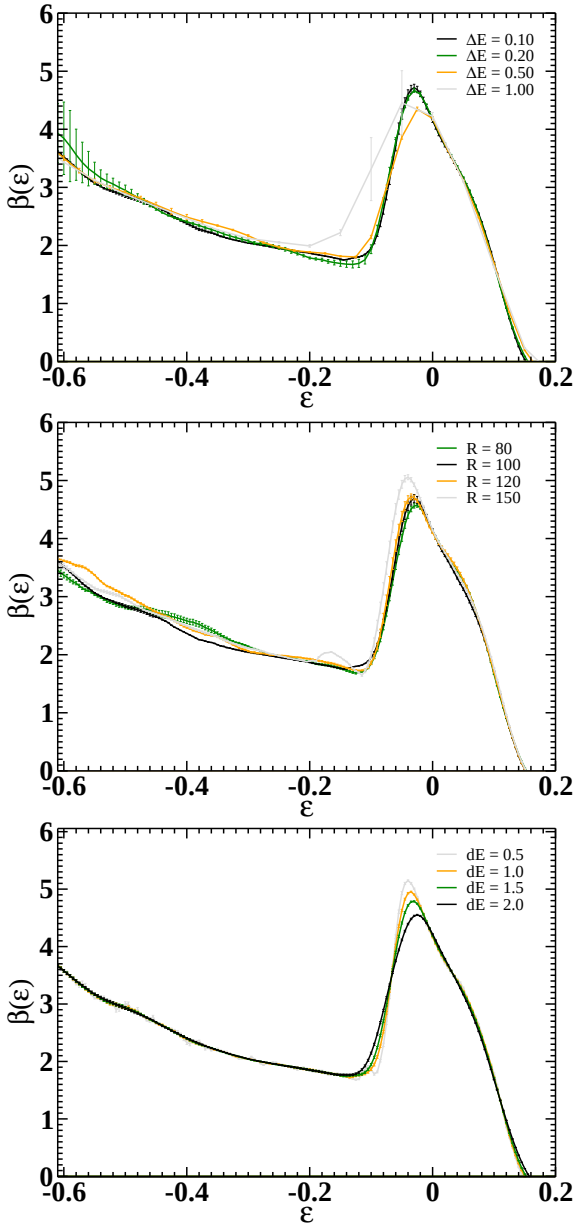

Figure 2. (Color online) Caloric curves for $2\times\mathrm{hIAPP}_{20-29}$ as a function of energy (E) per residue $\varepsilon = E/N$ as an illustration of various error-sources in microcanonical simulations. Upper Panel: energy bin-size effects for $\triangle E = 0.1$ in black (black), $\triangle E = 0.2$ in green (dark gray), $\triangle E = 0.5$ in orange (gray), and $\triangle E = 1.0$ in light gray (light gray). Central Panel: finite-volume effect as a function of linear size of container radius for $R = 80$ in green (dark gray), $R = 100$ in black (black), $R = 120$ in orange (gray), and $R = 150$ in light gray (light gray). Lower Panel: kernel-size effects in finite difference derivatives for $dE = 0.5$ in light gray (light gray), $dE = 1.0$ in orange (gray), $dE = 1.5$ in green (dark gray), and $dE = 2.0$ in black (black).

Upper Panel of Fig. (2), where one perceives the coarsening effects induced by $\triangle E$ in a region in the vicinity of the phase transition. In general, the peak of $\beta(\varepsilon) \times \varepsilon$ was shifted by no more than 6% when considering the extreme values of the bins here employed.

Following, by fixing $\triangle E = 0.1$ we have investigated, along about 300 MUCA runs, the effect of taking different radius R in our simulations. Analogously to our previous analysis we have obtained $E_{ground} = \{-20.21, -18.68, -17.59, -19.59\}$ when taking $R = \{80, 100, 120, 150\}$. The fluctuation of energy values found as ground-states as a function of increasing volumes is compatible with an unbiased statistical fluke, so presenting no systematics. Also, except by an exceptional 5% deviation on the height of the peak of $\beta(\varepsilon) \times \varepsilon$ — implying on a small shift on its energy location $\Delta\varepsilon/\varepsilon < 1\%$ — seen when $R = 150$, all curves physically match. Additionally, it also deserves to be noted that the smaller container we employed has a linear extension about 20-times larger than fully-distended peptides here simulated. Thus, as observed in the Central Panel of Fig. (2), volume independence of our aggregation studies seems us as a plausible working hypothesis.

The effects of finite-difference derivatives on data analysis was checked by considering the output from a full-scale MUCA simulation, performed using $\triangle E = 0.1$, $R = 100$ and 1000 MUCA iterative runs each one taking 10^7 MC-steps. Here derivatives of $S(E)$ were computed as central finite-diferences dE for $n-$point kernels, which is translated on our setup as $n = \{5, 10, 15, 20\} \longleftrightarrow dE = \{0.5, 1.0, 1.5, 2.0\}$. Results observed [in the Lower Panel of Fig.(2)] for $\beta(\varepsilon)$ clearly shows that employing relatively small kernel sizes (e.g $5 \leq n \leq 15$) may notably improve signal-to-noise levels when computing (high-order) derivatives of $S(E)$, at the expense of introducing some systematics in highly-curved regions. More interestingly, despite of gradually incrementing the kernel size from $n = 5$ up to $n = 15$ — which is able to fully-supress most statistical noise — it only induces a maximal $7(1)\%$ shift on the height of the peak of $\beta(\varepsilon) \times \varepsilon$. Thus, while using this technique is mandatory to compute quantities as Eq.(6), the determination of transition temperatures as in Section III may be more successful by not employing Maxwell's constructions over caloric curves, but by using "shifted entropies" [20]. Hence, in such approach one has just to iteratively operate directly on $S(\varepsilon)$ by numerically searching for β_c while imposing the physical constraint: $H(\varepsilon)|_{\varepsilon=\varepsilon_{frag}} \equiv H(\varepsilon)|_{\varepsilon=\varepsilon_{agg}} = \left[\varepsilon - \beta_c^{-1} S(\varepsilon)\right]\big|_{\varepsilon=\varepsilon_c}$. Which is equivalent to say that at the temperature of transition β_c^{-1} the free energy $H(\varepsilon)$ on Eq.(7) has an equal and double degenerated minimum.

[1] S. Melmed *et* al., *Williams textbook of endocrinology* (Elsevier/Saunders, 2011); American Diabetes Society, http://www.diabetes.org/

[2] P. Zhang *et* al., Diabetes Res. and Clin. Pract. **87**, 293 (2010).

[3] P. Westermark *et* al., Proc. Natl. Acad. Sci. USA **84**, 3881 (1987); Proc. Natl. Acad. Sci. USA **87**, 5036 (1990).

[4] R. L. Hull *et* al., J. Clin. Endocrinol. Metab. **89(8)**, 3629 (2004).

[5] A. Lorenzo *et* al., Nature **368**, 756 (1994).

[6] C. M. Dobson, Nature **426**, 884 (2003).

[7] F. Chiti *et* al., Nature **424**, 805 (2003).

[8] D. Chandler, Nature **437**, 640 (2005).

[9] J. N. Onuchic, Z. Luthey-Schulten and P. G. Wolynes, Annu. Rev. Phys. Chem. **48**, 545 (1997).

[10] V. Tozzini, Curr. Opin. in Struct. Bio. **15**, 144 (2005); C. Wu and J.-E. Shea, Curr. Opin. in Struct. Biol. **21**, 209 (2011).

[11] D. H. E. Gross, *Microcanonical Thermodynamics,* World Scientific, Singapore (2001).

[12] J. Hernandez-Rojas, and J. M. Gomez Llorente, Phys. Rev. Lett. **100**, 258104 (2008).

[13] C. Junghans, M. Bachmann, and W. Janke, Phys. Rev. Lett. **97**, 218103 (2006).

[14] B. A. Berg and T. Neuhaus, Phys. Lett. B **267**, 249 (1991); Phys. Rev. Lett. **68**, 9 (1992).

[15] F. H. Stillinger, T. Head-Gordon, and C. L. Hirshfeld, Phys. Rev. E **48**, 1469 (1993); F. H. Stillinger and T. Head-Gordon, Phys. Rev. E **52**, 2872 (1995).

[16] M.A. Roseman, J. Mol. Biol. **200**, 513 (1988).

[17] K. F. DuBay *et* al., J. Mol. Biol. **341**, 1317 (2004).

[18] O. Conchillo-Solé *et* al., BMC Bioinfo. **8**:65, (2007).

[19] S. Brown, N. J. Fawzi, and T. Head-Gordon, Proc. Natl. Acad. Sci. USA **100**, 10712 (2003).

[20] R. B. Frigori, L. G. Rizzi, and N. A. Alves, The Jour. of Chem. Phys. **138**, 015102 (2013).

[21] B. A. Berg, Fields Inst. Commun. **26**, 1 (2000); Comp. Phys. Comm. **153**, 397 (2003).

[22] T. Kennedy, J. Statist. Phys. **106**, 407 (2002).

[23] T. Christopeit *et* al., Prot. Sci. **14**, 2125 (2005).

[24] D. Sept, and J. A. McCammon, Biophys. Jour. **81**, 667 (2001).

[25] P. Hortschansky *et* al., Prot. Sci. **14**, 2915 (2005).

[26] U. H. Danielsson, M. Lundgren, and A. J. Niemi, Phys. Rev. E **82**, 021910 (2010).

[27] M. Chernodub, S. Hu, and A. J. Niemi, Phys. Rev. E **82,** 011916 (2010).

[28] B. Svetitsky, and L. Yaffe, Nucl. Phys. B **210**, 423 (1982).

[29] R. Fiore, A. Papa, and P. Provero, Phys. Rev. D **67**, 114508 (2003); R. B. Frigori, Nucl. Phys. B **833**, 17 (2010).

[30] F. Zantow, and O. Kaczmarek, BNL-75353-2006-CP; E. Gava, and R. Jengo, Phys. Lett. B **105**, 285 (1981).

[31] R. Falcone, R. Fiore, M. Gravina, and A. Papa, Nucl. Phys. B **785**, 19 (2007).

[32] V. M. Fokin, N. S. Yuritsyn, and E. D. Zanotto, *Nucleation Theory and Applications*, Wiley (2005).

[33] P. A. Hollander *et* al., Diabetes Care **26(3)**, 784 (2003).

[34] R. D. Murphy *et* al., Biophys. Chem. **167,** 1 (2012).

[35] W. M. Berhanu, and U. H. E. Hansmann, PLOS One **9(5)**, e97051 (2014).

[36] N.-V. Buchete, J. E. Straub, and D. Thirumalai, Proteins

70(1), 119 (2008).

[37] D. P. Landau, and K. Binder, *A Guide to Monte Carlo Simulations in Statistical Physics*, Cambridge University Press (2005); C. Gattringer, and C. B. Lang, *Quantum Chromodynamics on the Lattice*, Springer (2010).